Journal of The Electrochemical Society, **154** (10) B998-B1005 (2007)
0013-4651/2007/154(10)/B998/8/$20.00 © The Electrochemical Society

Liquid Water Formation and Transport in the PEFC Anode

Shanhai Ge and Chao-Yang Wang*,z

Electrochemical Engine Center (ECEC) and Department of Mechanical and Nuclear Engineering, The Pennsylvania State University, University Park, Pennsylvania 16802, USA

Transparent polymer electrolyte fuel cells (PEFCs) with parallel- and serpentine-channel flowfields have been developed to study liquid water formation and transport on the anode side. In situ observations reveal that liquid water in the anode channels results from condensation of water on cooler and more hydrophilic channel walls and that water available for condensation in the anode comes either from the cathode through membrane transport or from hydrogen consumption. No water droplets can be found on the anode gas diffusion layer (GDL) surface, in sharp contrast with the cathode side. Moreover, GDL wettability has much influence on water distribution in the anode for the cell operated at low current density (0.2 A/cm^2). Using hydrophobic GDL at low current density, water is prone to condense on the channel surfaces rather than inside hydrophobic carbon paper GDL. The condensed water then accumulates and results in channel clogging in the anode. In contrast, by using untreated carbon paper as the anode GDL, it is found that channel clogging by liquid water is avoided under similar operating conditions. This finding implies that water distributions in the anode with hydrophilic and hydrophobic anode GDLs differ much from each other at low current density. Finally, experiments suggest that water condensation on the channel surfaces is a primary mechanism for liquid water formation and anode flooding and that elevating the anode plate temperature modestly is effective to avoid surface condensation and mitigate anode flooding.
 [DOI: 10.1149/1.2761830]

Manuscript submitted April 26, 2007; revised manuscript received May 22, 2007. Available electronically July 31, 2007.

Water management is a key to ensuring high performance and durability of polymer electrolyte fuel cells (PEFCs). At low temperatures and/or low gas-flow rates, a PEFC is prone to flooding. On the cathode side, liquid water in the gas diffusion layer (GDL), microporous layer (MPL), and catalyst layer (CL) may hinder oxygen transport to the active surface of catalysts. Liquid water may also accumulate in and block the flow channel, referred to as channel flooding or channel clogging. In a single PEFC with multipass flowfield, channel clogging may lead to shutdown of reactant flow and therefore reduce cell performance. In a PEFC stack, channel clogging leads to a nonuniform, cell-to-cell reactant distribution. The issue of water distribution and transport in PEFC has been the subject of numerous experimental and theoretical studies.[1-6]

Prior experimental efforts to probe water distribution in an operating PEFC include optical visualization using transparent cells,[7-12] neutron radiography,[13,14] magnetic resonance imaging (MRI),[15,16] and X-ray microtomography.[17,18] Due to excellent spatial and temporal resolution, optical visualization is a powerful and convenient method particularly suited for studying two-phase flow regimes in flow channels. Optical visualization has been widely employed to study liquid water flow in channels and microdroplet behavior on the GDL as well as CL surfaces.[7,8,10,11] Zhang et al.[9] demonstrated that there are two modes of liquid water removal from the cathode GDL surface, one through droplet detachment by shear force of gas flow in the channel and the other by capillary wicking onto the more hydrophilic channel walls followed by the annular film flow and/or liquid slug flow in the channel. Despite extensive efforts, neutron radiography has yet to separate anode water from cathode water or to distinguish liquid water in different layers, making it useful to study water management in a PEFC.[19] MRI has not been applied to probe liquid water in CL or GDL because carbon-based components in PEFCs are magnetically inductive. More recently, X-ray microtomography[17,18] was successfully developed to quantify the liquid water saturation distribution in cathode GDL during gas purge as well as under load.

Whereas all the literature efforts have focused exclusively on cathode flooding in a PEFC as it is a water-generating electrode, the present work aims to shed light on liquid water formation and transport on the anode side of the PEFC for the first time. Although the anode does not generate water per se, anode flooding has serious consequences to PEFC operation and durability for several reasons: (*i*) anode flooding may lead to localized fuel starvation and consequently carbon corrosion in the cathode CL,[20] (*ii*) liquid water, once accumulated in the anode channels, is much less likely to be removed by the anode gas flow due to exceedingly low flow rate, and (*iii*) it is inconvenient to separate liquid water out of the residual fuel exiting from a PEFC through a recirculation loop under automotive conditions.

In this work, we present anode visualization results, pressure drop, and water balance data under certain operating conditions in order to elucidate the liquid water formation and transport mechanism in the anode of a PEFC. In addition, the influence of anode GDL wettability is investigated.

Experimental

The cell structure for these experiments is similar to that in previous works.[8-11] In brief, a catalyst-coated membrane (CCM, 30 μm thick Gore membrane) was sandwiched by anode and cathode GDL. The anode GDL was polytetrafluoroethylene (PTFE)-proofed carbon paper with MPL or untreated carbon paper (Toray TGP-H-060). The cathode GDL was PTFE-proofed carbon paper with MPL. Two gold-plated stainless steel current-collector plates were machined to form flowfields (1 mm in width, 0.5 mm in depth). A transparent polycarbonate plate was placed outside of the anode current-collector plate for optical access. The polycarbonate plate and cathode current collector were clamped between two stainless steel end plates. A window was machined on the anode end plate. The width of the rib (land) was 1 mm. The Pt loadings in the anode and cathode catalyst layers were both 0.4 mg/cm^2. Two kinds of flowfields were used in this work, a seven-pass parallel-channel with an electrode active area of 14 cm^2 and a four-pass serpentine channel with an active area of 5 cm^2.

The cell was tested using a fuel cell test station (Teledyne). Exit pressures of the anode and the cathode were both kept at 2 or 1 atm (absolute). To accurately control the cell temperature, the cathode end plate has a built-in metal heat exchanger with circulating water from a constant temperature bath (Fisher Scientific), and a rod header was placed in the anode end plate and a thermocouple was inserted in the transparent polycarbonate plate to monitor the anode plate temperature. The cell was preconditioned by operating with water-saturated hydrogen and air and with low stoichiometric ratios at 80°C for 6 h.

Current densities used in this study are 0.2, 0.5, and 0.8 A/cm^2. Cell temperatures are 50 and 80°C. The hydrogen stoichiometric ratio ranges from 1.5 to 4.0. Cell voltage, anode pressure drop (Rosemount 3051 pressure transmitter), and high-frequency cell impedance (at 1 kHz, Agilent 4338B AC milliohm meter) were re-

* Electrochemical Society Active Member.
z E-mail: cxw31@psu.edu

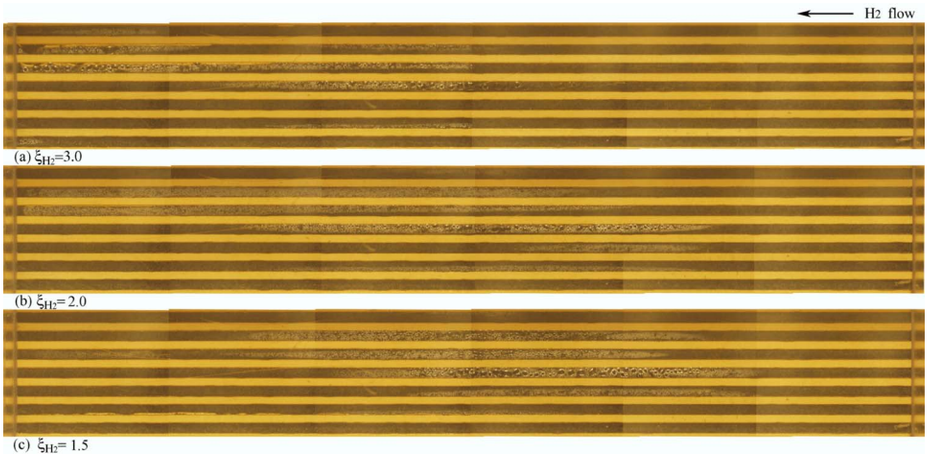

Figure 1. (Color online) Images of the anode side of a seven-channel, 14 cm^2 cell for various anode stoichiometric ratios. PTFE-proofed carbon paper is used as anode GDL. (i = 0.2 A/cm^2, T_{cell} = 80°C, $RH_{H_2} = RH_{air}$ = 66%, ξ_{air} = 3.0, $p_{H_2} = p_{air}$ = 2 atm, t = 60 min.)

corded and images (Olympus DP 70 digital camera, up to 12 megapixel color images, Navitar zoom lens) were taken at different times. Before recording these parameters under specific conditions, both sides of the cell were purged to remove water droplets and/or film in flow channels. The flow rates of the anode and cathode purging gases were 1.0 and 2.5 L/min, respectively, with purge duration of 2 min. To calculate the net water-transport coefficient through the membrane from the anode to cathode, a water moisture trap containing anhydrous calcium sulfate (W.A. Hammond Drierite Co., Ltd.) was connected to the anode exit to collect water in the hydrogen exhaust, with a 3–8 h time interval for water collection.

Results and Discussion

Parallel-channel flowfield.— A series of experiments was carried out under the above-mentioned conditions for three current densities: 0.2, 0.5, and 0.8 A/cm^2. In this work, the cells with seven-pass parallel flow channel were all operated in the counterflow mode. Figure 1 shows images of the anode side of the cell operated at current density of 0.2 A/cm^2 and at different hydrogen stoichiometric ratios. Anode and cathode inlet relative humidities (RHs) were both kept at 66%. PTFE-proofed carbon paper with MPL was used as anode GDL. The images were all taken 60 min after the start of the experiments. It is seen that water droplets and films appear in the anode channel for the cell operated at low current density (0.2 A/cm^2). The images at different hydrogen stoichiometric ratios show similarities. Because the operating time was not long enough, water clogging was not observed. In addition, a certain volume of liquid is required for clogging to occur. On the anode side, the rate of liquid water formation is very low compared to the cathode side, as water must either come from the cathode side through the membrane or condense from the anode gas at a small flow rate due to hydrogen consumption. Therefore, it takes much longer for the anode to accumulate a threshold volume of liquid water that causes channel clogging.

When the current density was set to 0.5 or 0.8 A/cm^2 and other operating conditions (T_{cell} = 80°C, $RH_{H_2} = RH_{air}$ = 66%, ξ_{H_2} = 1.5–3.0, ξ_{air} = 3.0, $p_{H_2} = p_{air}$ = 2 atm, t = 60 min) are the same (as in Fig. 1), no water droplets and films were observed in the anode flow channels. This indicates that anode flooding is strongly controlled by current density.

The location of water droplets in the anode flow channels can be identified by different lighting methods. Figure 2 shows images taken using two lighting techniques for the cell operated at a current density of 0.2 A/cm^2. Anode and cathode inlet RH were kept at 26 and 66%, respectively. Image (a) was taken when illuminating light was turned on directly perpendicular to the transparent window. Image (b) was taken when this direct light was shut off and only background light was used with longer exposure time. Because of the unique reflection pattern between a direct light on a water droplet, the exact location of water droplets can be discerned, showing that water droplets exist on the transparent window or channel surface instead of the GDL surface. Three regions (land, current collector depth, and GDL surface) are shown on these pictures. Some water droplets are in the front of the region of current collector depth. Using this background lighting technique, it was found that no water droplets formed on the anode GDL surface under any operating conditions investigated in this work. This finding clearly demonstrates that the liquid water accumulated in the anode channel does not directly come from the anode GDL in liquid form. Thus, the only source of liquid water in the anode channel is the water flux from the anode GDL in the vapor phase followed by water condensation on channel surfaces. The surface condensation is caused by either cooler or more hydrophilic channel walls or by hydrogen consumption that causes supersaturation in the diminishing anode gas. The latter factor can be studied by varying the hydrogen stoichiometric ratio, particularly for the stoichiometric ratio close to unity, as is described later.

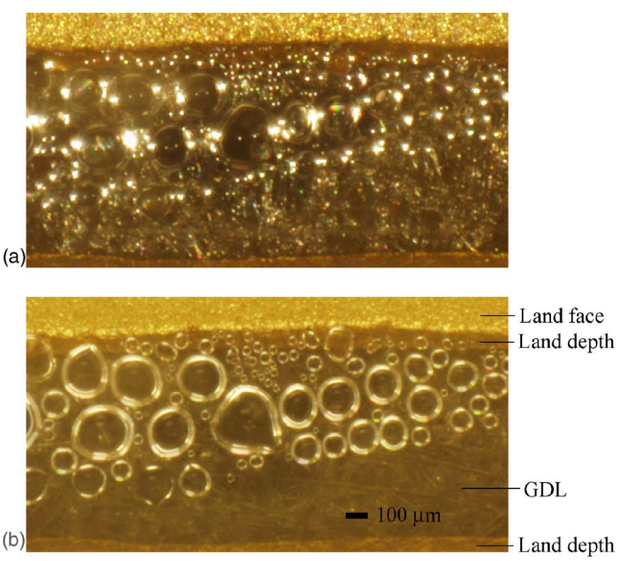

Figure 2. (Color online) Comparison of water droplet images taken by (a) front lighting and (b) background lighting. PTFE-proofed carbon paper is used as anode GDL. The view is in the center portion of the flowfield. (i = 0.2 A/cm^2, T_{cell} = 80°C, RH_{H_2} = 26%, RH_{air} = 66%, ξ_{H_2} = 2.0, ξ_{air} = 3.0, $p_{H_2} = p_{air}$ = 2 atm, t = 60 min.)

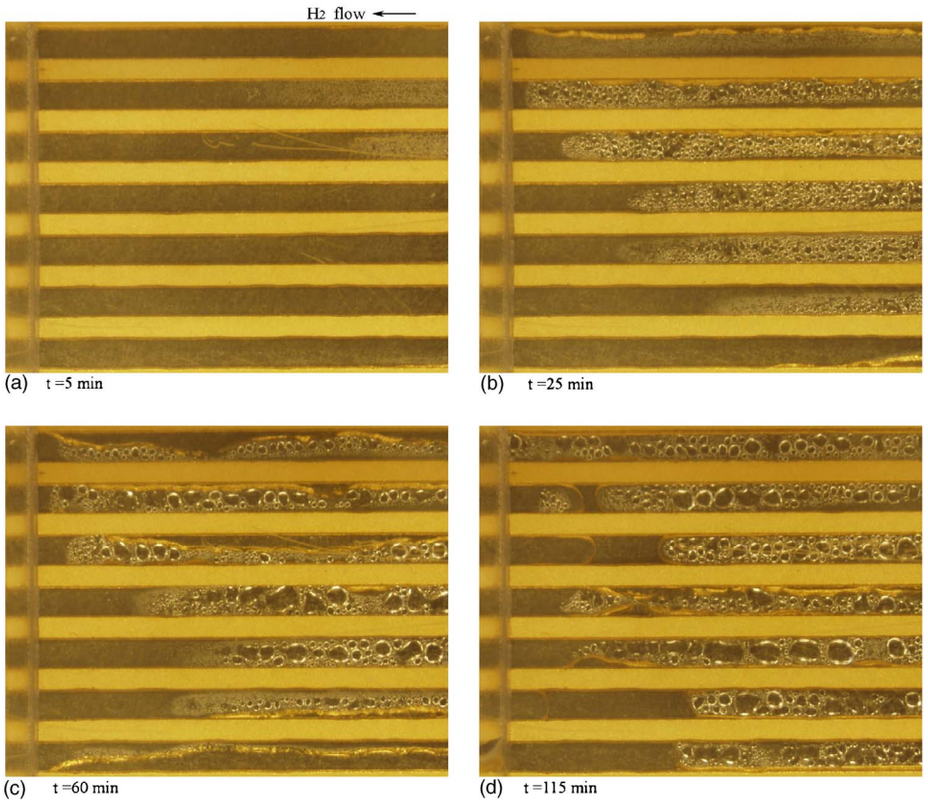

Figure 3. (Color online) Sequential images of water droplets and films in the anode. PTFE-proofed carbon paper is used as anode GDL. The view is in the outlet portion of the flowfield. (i = 0.2 A/cm^2, T_{cell} = 80°C, $RH_{H_2} = RH_{air}$ = 66%, $\xi_{H_2} = \xi_{air}$ = 2.0, $p_{H_2} = p_{air}$ = 2 atm.)

The rate of liquid water formation from condensation is very low. Based on this reasoning, we did an experiment with a longer operational time (2 h) to investigate anode-channel clogging. Figure 3 shows sequential images of water droplets and films in the anode taken at different time intervals. PTFE-proofed carbon paper with MPL was used as anode GDL. The view is in the outlet portion of flowfield. These sequential images show that some water droplets appeared on the transparent plate when operating time reached 5 min, and that these small water droplets were found to grow and accumulate with time. When the operating time reached 25 min, the size of water droplets were seen to be 50–400 μm and water films were seen on the current collector surface in some flow channels. When it reached 60 min, some water droplets on the transparent plate enlarged to 800 μm and some water films occupied the flow channel to 80% but no channel clogging was observed. However, with operating time up to 115 min, 4 channels (the 2nd, 3rd, 6th, and 7th channels from the top) were clogged by liquid water because the hydrogen flow rate is too low to remove these water columns.

The anode pressure drop was recorded simultaneously during this 2 h experiment. Figure 4 shows the variation of the anode pressure gradients with time. The operating conditions are the same as in Fig. 3, with 1 min time interval for measuring the pressure drop. The channel length is 0.1 m. The anode pressure gradient of the cell with hydrophilic GDL under identical operating conditions is also shown. It is found that the anode pressure gradient of the cell with hydrophobic anode GDL increases slowly in the first 60 min of the experiment. From 60 to 120 min of the operation, the anode pressure gradient increases rapidly. This is because some channels were blocked by liquid water (the 2nd, 3rd, 6th, and 7th channels from the top) and some channels (the 1st, 4th, and 5th channels from the top) became narrow in flow cross sections. The pressure gradient data agrees well with the visualization result shown in Fig. 3.

The fact that liquid water observed in anode flow channels results from vapor condensation was further confirmed by experiments carried out at a lower temperature. Figure 5 shows in situ images of the anode side for the cell operated at 50°C and 0.2 A/cm^2. PTFE-proofed carbon paper with MPL was used as anode GDL. Both images were taken at 60 min after the start of the experiment. When the relative humidity of inlet hydrogen is high (78%), hydrogen becomes oversaturated with water at 17% of the total channel length due to hydrogen consumption. Even when dry hydrogen is fed to the cell, the anode gas stream becomes oversaturated with water at 35% of the total channel length, followed by water condensation in the anode channel. In both experiments carried out at 50°C, water drop-

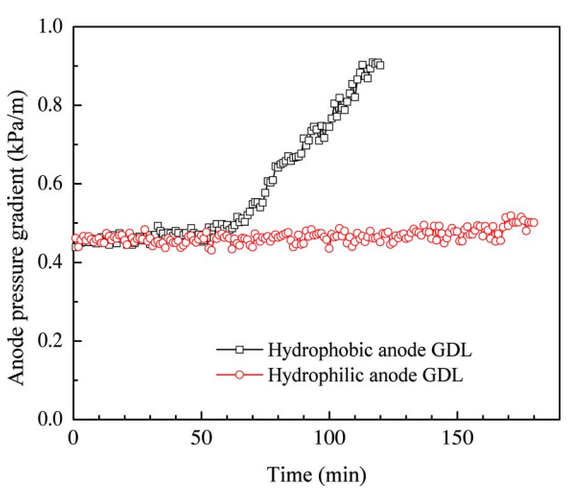

Figure 4. (Color online) Comparison of anode pressure gradients of the cells using different GDLs. (i = 0.2 A/cm^2, T_{cell} = 80°C, $RH_{H_2} = RH_{air}$ = 66%, $\xi_{H_2} = \xi_{air}$ = 2.0, $p_{H_2} = p_{air}$ = 2 atm.)

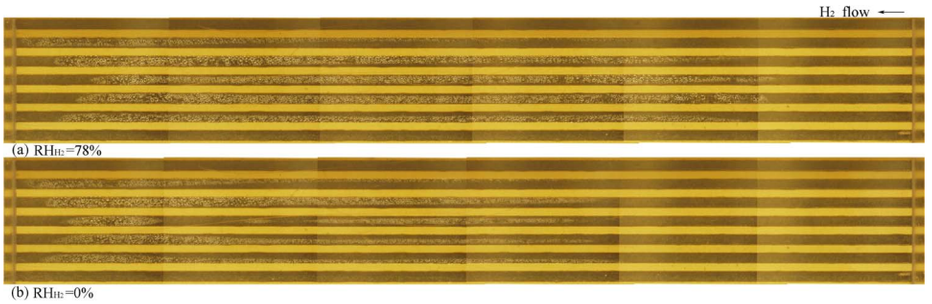

Figure 5. (Color online) Images of the anode side of the cell with different anode RHs. PTFE-proofed carbon paper is used as anode GDL. (i = 0.2 A/cm^2, T_{cell} = 50°C, RH_{air} = 78%, ξ_{H_2} = 2.0, ξ_{air} = 3.0, $p_{H_2} = p_{air}$ = 1 atm, t = 60 min.)

lets and films were observed on the transparent plate surface and current collector surface, respectively. No liquid water was observed on the GDL surface.

Figure 6 shows in situ images of the anode side of the cell at different hydrogen stoichiometric ratios. The operating conditions are the same as in Fig. 1. However, in this set of experiments, untreated carbon paper was used as anode GDL and no MPL was coated on the GDL. This untreated carbon paper does not contain PTFE and it is hydrophilic. The images were all taken at 60 min after the start of each experiment. Similar to the results using hydrophobic anode GDL, it is seen that water droplets and films appear on the anode side for the cell operated at 0.2 A/cm^2. The images taken at different hydrogen stoichiometric ratios are similar to each other, indicating that hydrogen flow rates investigated have negligible influence on liquid water formation and transport in the anode.

To further explore water transport formation in the anode and the effect of GDL wettability on water transport, an experiment using untreated carbon paper as anode GDL was carried out for 3 h. Figure 7 shows sequential images of water droplets and films on the anode at 0.2 A/cm^2 taken at different time intervals. The view is in the outlet portion of the flowfield. Stoichiometric ratios of hydrogen and air were both 2.0. Similar to the result using hydrophobic anode GDL, some water droplets appeared on the transparent plate when the operating time reached 5 min. These small water droplets also grew and accumulated with time. With operating time up to 25 min, a large water drop about 4 mm in length was found in the bottom channel. It enlarged to 9 mm in length after 60 min elapsed. When this drop was large enough, it contacted the hydrophilic GDL. The hydrophilic GDL absorbed this water drop and its size decreased at 90 min, as shown in Fig. 7d. When the operating time reached 115 min, this water drop was completely absorbed by the GDL and new water droplets appeared on the transparent plate surface. No channel clogging was observed over the 180 min period when hydrophilic GDL was used on the anode side. Again, this suggests that liquid water stays in the anode gas channels when the GDL is hydrophobic but is wicked into the GDL when the anode GDL is hydrophilic. Nonetheless, it is unclear exactly what increase in liquid water saturation exists inside a hydrophilic GDL compared to a hydrophobic GDL. If the water saturation is exceedingly high inside the anode GDL, there could be a problem of local fuel starvation.

The anode pressure gradient during the above-mentioned 180 min experiment using hydrophilic anode GDL was shown in Fig. 4. The pressure gradient increases from 0.46 kPa/m initially to 0.50 kPa/m at termination. In contrast, the pressure gradient increases beyond 0.90 kPa/m within 120 min if using a hydrophobic anode GDL. The anode pressure gradient confirms that using hydrophilic anode GDL can prevent channel clogging and hence localized fuel starvation, which can lead to carbon corrosion in the cathode catalyst layer.

Serpentine-channel flowfield.— Liquid water formation and transport in the anode of PEFCs is further investigated using a four-pass serpentine flowfield with 0.07 m channel length. The cells with four-pass serpentine flow channels were all operated in the coflow mode. In this work, air inlet RH is kept high so that different flow configurations have little influence on liquid water formation in the anode. Again, two kinds of anode GDL were used, one PTFE-proofed carbon paper with MPL (hydrophobic GDL) and the other untreated carbon paper (hydrophilic GDL). Figure 8 shows cell potentials and anode pressure gradients of the cells with four-pass serpentine flowfield at different hydrogen stoichiometric ratios. In these experiments, the hydrogen stoichiometric ratios were set to 4.0, 3.0, 2.0, and 1.5, and air stoichiometric ratio was kept at 3.0. The cell was operated at 0.2 A/cm^2 for 6 h. Similar to the results using parallel-channel flowfield, the anode pressure gradient increased slightly with time in the first 180 min interval when untreated carbon paper was used as anode GDL. After about 180 min, the anode pressure became stable. When PTFE-proofed carbon paper with MPL was used as anode GDL, the anode pressure gradient increased significantly after 60 min. Again, this confirms that anode

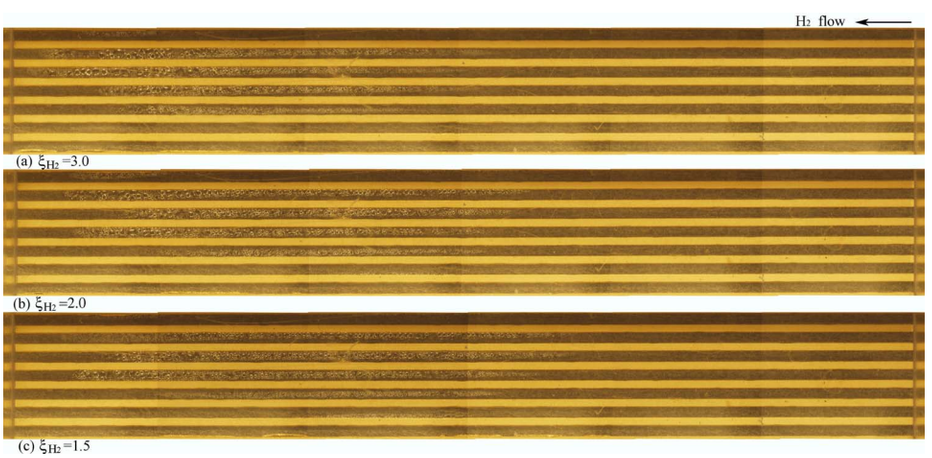

Figure 6. (Color online) Images of the anode side of the cell for various anode stoichiometric ratios. Untreated carbon paper is used as anode GDL. (i = 0.2 A/cm^2, T_{cell} = 80°C, $RH_{H_2} = RH_{air}$ = 66%, ξ_{air} = 3.0, $p_{H_2} = p_{air}$ = 2 atm, t = 60 min.)

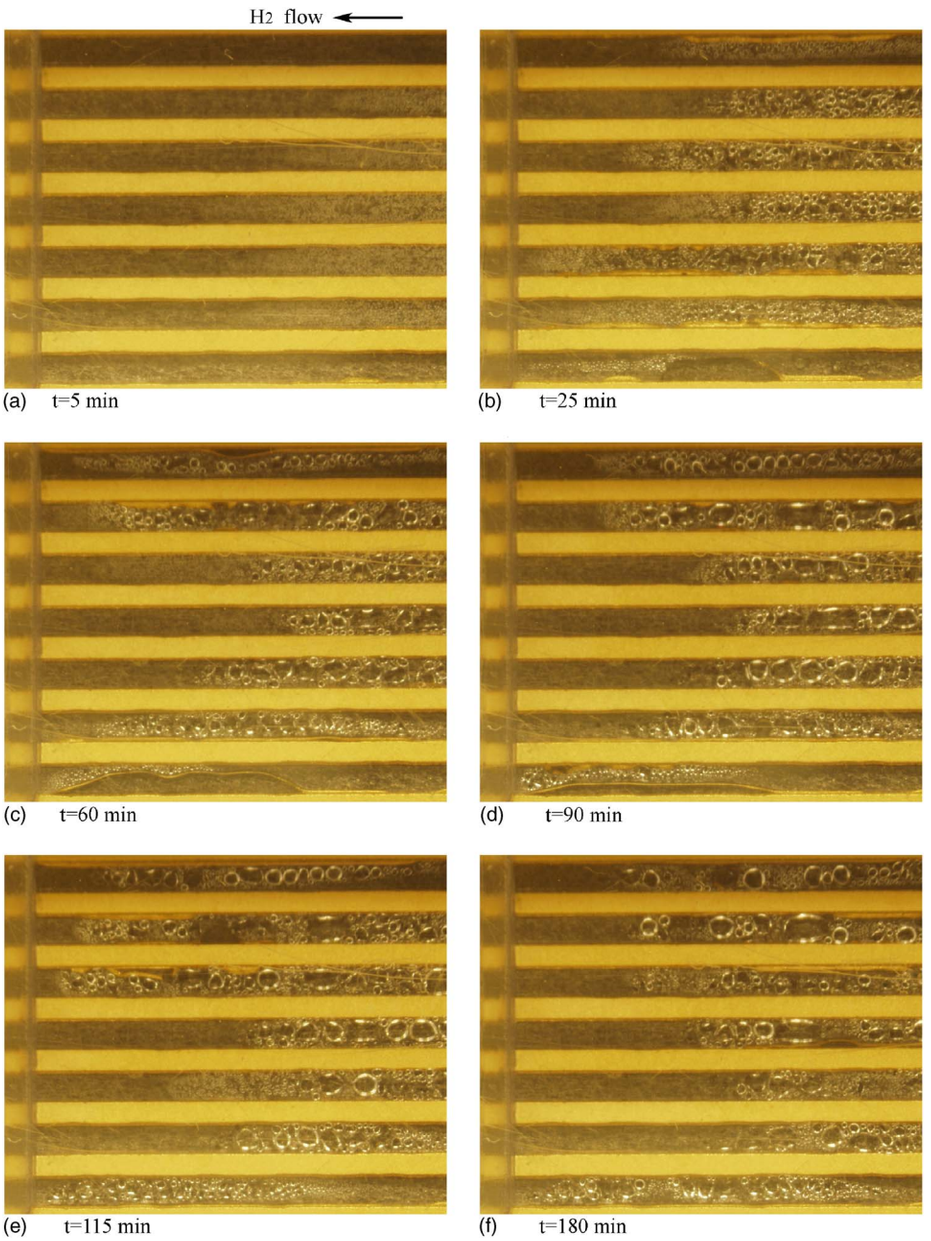

Figure 7. (Color online) Sequential images of water droplets and films in the anode. Untreated carbon paper is used as anode GDL. The view is in the outlet portion of the flowfield. (i = 0.2 A/cm^2, T_{cell} = 80°C, $RH_{H_2} = RH_{air}$ = 66%, $\xi_{H_2} = \xi_{air}$ = 2.0, $p_{H_2} = p_{air}$ = 2 atm.)

channel clogging leads to sharply increased pressure gradient. Therefore, anode pressure gradient may be used to diagnose anode channel clogging.

Figure 8 also shows that at the same current density of 0.2 A/cm^2, the average cell potential using hydrophobic anode GDL is about 5 mV higher than that using hydrophilic anode GDL. The main reason is that the internal resistance of the cell with hydrophilic GDL (152 mΩ/cm^2 at 50°C and 0.2 A/cm^2) is larger than that with hydrophobic GDL (126 mΩ/cm^2 at 50°C and 0.2 A/cm^2), because the untreated GDL is not coated with MPL and consequently there is a high contact resistance between GDL and CL. The cell potentials stay relatively stable over time at each hydrogen stoichiometric ratio investigated. Moreover, the hydrogen stoichiometric ratio has almost no influence on the cell performance. This indicates that anode channel clogging and water remaining in the hydrophilic GDL have not influenced the anode kinetics due to facile hydrogen diffusion.

Figures 9 and 10 show in situ images of the anode side of the cells with four-pass serpentine flowfield for the cells operated at 0.2 A/cm^2. Both images were taken at the 180 min point. Using hydrophobic anode GDL, water droplets on the transparent plate and water films on the land surface were observed, and three of the four flow channels (the 2nd, 3rd, and 4th channels from the left) were blocked by liquid water. Using hydrophilic anode GDL, water droplets on the transparent plate and water films on the land surface were observed, with no observable channel clogging. No water droplets were observed on the GDL surface in either experiment.

Water balance measurements.— In this work, a thin membrane (30 μm thick Gore membrane) was used. A thin membrane favors water back diffusion and consequently the anode outlet may become oversaturated. Figure 11 shows the RH of hydrogen gas exiting the cell and net water-transport coefficient through the membrane as functions of the hydrogen stoichiometric ratio. The cells with four-pass serpentine flow channels were operated in the coflow mode using hydrophobic and hydrophilic anode GDLs. It can be seen from

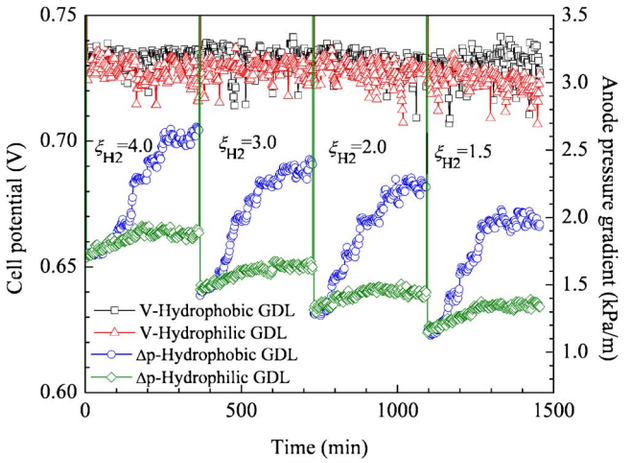

Figure 8. (Color online) Cell potentials and anode pressure gradients of the cells with four-pass serpentine flowfield. (i = 0.2 A/cm^2, T_{cell} = 50°C, $RH_{H_2} = RH_{air}$ = 78%, ξ_{air} = 3.0, $p_{H_2} = p_{air}$ = 1 atm.)

Fig. 11a that at 0.2 A/cm^2 the outlet gas is oversaturated, resulting in water droplets or water clogging in the anode channel, as shown in Fig. 9 and 10. The RH of outlet hydrogen using hydrophilic anode GDL is lower than that using hydrophobic anode GDL because the hydrophilic anode GDL may retain some liquid water. At 0.5 A/cm^2, the hydrogen stoichiometric ratio and anode GDL wettability have almost no influence on the RH at the anode outlet. The RHs of the outlet gas are both about 100%. The image shows no liquid water in the anode flow channel for the cell operated at 0.5 A/cm^2. At 0.8 A/cm^2, the anode outlet becomes undersaturated and consequently no liquid water was observed in the anode flow channel. If no liquid water is present in the anode, anode GDL wettability should have no influence on liquid water distribution.

In fluorinated membranes, water is transported by electro-osmotic drag, back diffusion, and permeation.[1,21] In this work, no

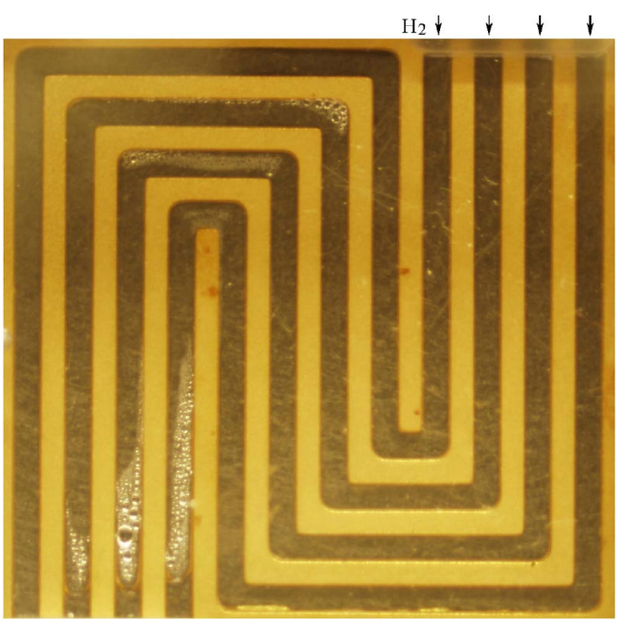

Figure 9. (Color online) Image of the anode side of the cell with four-pass serpentine flowfield. PTFE-proofed carbon paper is used as anode GDL. (i = 0.2 A/cm^2, T_{cell} = 50°C, $RH_{H_2} = RH_{air}$ = 78%, $\xi_{H_2} = \xi_{air}$ = 3.0, $p_{H_2} = p_{air}$ = 1 atm.)

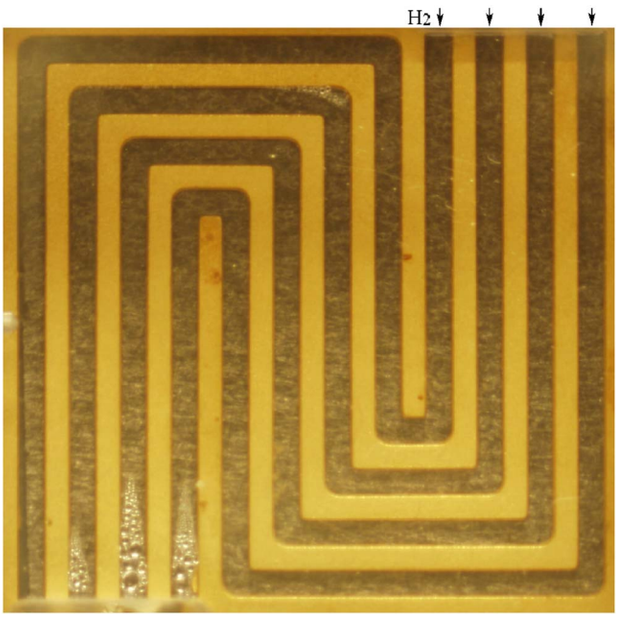

Figure 10. (Color online) Image of the anode side of the cell with four-pass serpentine flowfield. Untreated carbon paper is used as anode GDL. (i = 0.2 A/cm^2, T_{cell} = 50°C, $RH_{H_2} = RH_{air}$ = 78%, $\xi_{H_2} = \xi_{air}$ = 3.0, $p_{H_2} = p_{air}$ = 1 atm.)

pressure difference exists between the anode and cathode. The net water flux through the membrane (N_w, mol/m^2 s) can thus be written as

$$N_w = \alpha \frac{i}{F} = n_d \frac{i}{F} - D_w c_f \frac{d\lambda}{dy} \quad [1]$$

where α is the net water-transport coefficient, i is the local current density, F is the Faraday constant, D_w is the water diffusivity in the membrane, c_f is the fixed charge concentration in the hydrated membrane, λ is the water content of the membrane, and y is the coordinate across the membrane. The net water-transport coefficient can be determined by measuring the molar flow rates of water entering ($F_{w,in}$, mol/s) and leaving the anode ($F_{w,out}$, mol/s)

$$\alpha \frac{i}{F} = \frac{F_{w,in} - F_{w,out}}{A} \quad [2]$$

where A is the electrode area. Figure 11b shows that the net water-transport coefficient is negative for the cell operated at 0.2 A/cm^2, meaning that water transports from the cathode to anode at a rate that increases with hydrogen stoichiometric ratio. The main reason is that back diffusion is sufficient to balance electro-osmotic drag at 0.2 A/cm^2 and the water content of the membrane at the anode CL/membrane interface is somewhat higher than that in contact with saturated vapor. When undersaturated hydrogen gas flows along the flowfield, water evaporates from the anode CL and then diffuses to the anode channel. The higher the hydrogen flow rate, the more water is removed by the anode flow.

Figure 11b also shows that the rate of water transport from the cathode to anode using hydrophilic anode GDL is lower than that using hydrophobic anode GDL at 0.2 A/cm^2, because the hydrophilic anode GDL retains some liquid water, thereby increasing the electro-osmotic drag coefficient[22] and reducing the rate of back diffusion.

Effect of higher anode plate temperature.— To further confirm the condensation mechanism for liquid water formation on the anode channel surface, some experiments were carried out by setting the anode plate temperature 2°C higher using the 5 cm^2 cell, with

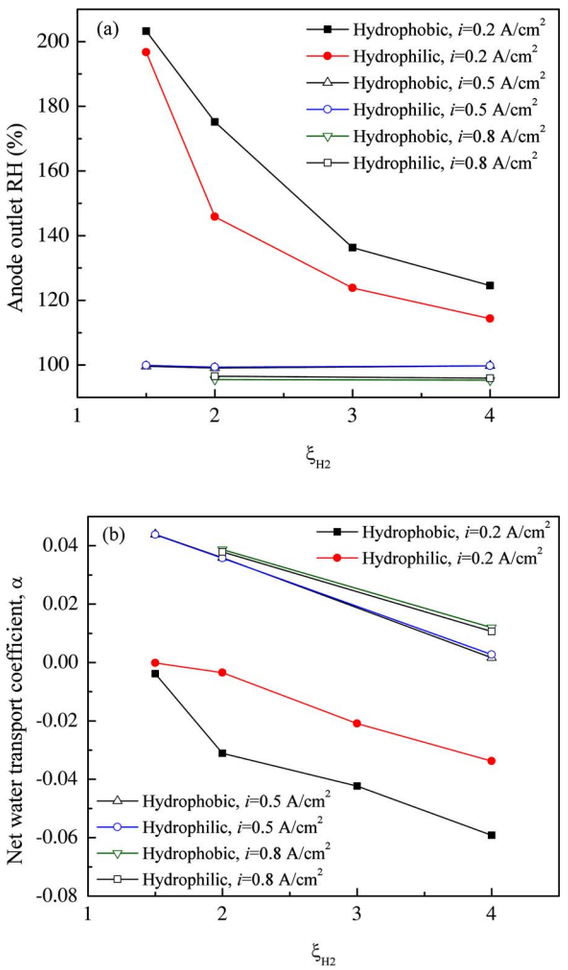

Figure 11. (Color online) Effects of current density on (a) RH of the outlet hydrogen and (b) net water transport coefficient. ($T_a = T_c = 50°C$, $RH_{H_2} = RH_{air} = 78\%$, $\xi_{H_2} = \xi_{air} = 3.0$, $p_{H_2} = p_{air} = 1$ atm.)

current density set to 0.2 A/cm^2. Figure 12 shows the effects of higher anode plate temperature on relative humidity of the outlet gas and the net water-transport coefficient. It can be seen that the relative humidity at the outlet remained constant and close to 100% (or equivalently 13.7 kPa water partial pressure) under all anode stoichiometric ratios and for both types of anode GDL, while the case with equal anode plate temperature shows oversaturation at the anode exit and the outlet RH (or water partial pressure) increases with decreasing hydrogen stoichiometry (see Fig. 11a). This comparison clearly indicates a single-phase behavior in the anode when the anode plate temperature is raised only slightly to avoid surface condensation. Corresponding images (not shown here) indeed confirm that liquid water in the anode channel vanishes at 0.2 A/cm^2 with 2°C higher anode plate temperature. These experiments therefore support the condensation mechanism for liquid water formation in the anode and suggest that elevating the anode plate temperature modestly is an effective method to mitigate anode flooding.

Schematic of liquid water formation.— Figure 13 schematically summarizes the mechanism for liquid water formation in the anode. The primary source of liquid water is condensation of water vapor brought into the fuel cell by hydrogen gas as hydrogen is consumed. There is some water transported through the membrane from the cathode; however, this is a relatively small source according to water-balance measurements. The condensation of water vapor in the anode channels occur preferentially over hydrophilic and cooler

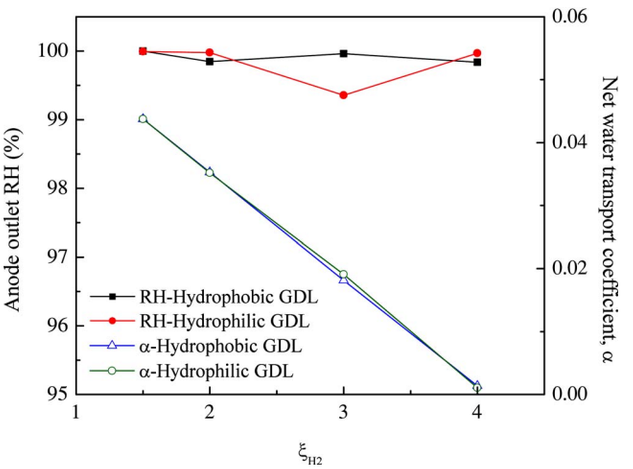

Figure 12. (Color online) Effect of 2°C higher anode plate temperature on RH at the anode outlet and the net water transport coefficient. (i = 0.2 A/cm^2, T_a = 52°C, T_c = 50°C, $RH_{H_2} = RH_{air}$ = 78%, $\xi_{H_2} = \xi_{air}$ = 3.0, $p_{H_2} = p_{air}$ = 1 atm.)

channel walls rather than the hydrophobic, warmer GDL. This is schematically shown in Fig. 13a. In actual automotive fuel cell stacks, surface condensation is promoted in lower temperature regions that interface with a coolant inlet. The liquid water accumulates and expands in volume, eventually clogging the gas channel when hydrophobic GDL is used, as shown in Fig. 13b. If untreated carbon paper is used as anode GDL, this hydrophilic GDL can wick liquid water accumulated in the anode flow channel, as shown in Fig. 13c. Therefore, a smaller degree of water clogging is observed under similar operating conditions.

These identified mechanisms for liquid water formation and transport in the anode are being incorporated into a comprehensive M2 model for PEFCs to enhance predictability of the anode operation.[1,4,6,23-25]

Conclusion

GDL wettability plays an influential role in liquid water transport and distribution in the anode. Using hydrophobic GDL at low current density (0.2 A/cm^2), water is prone to condense on the channel walls rather than inside the hydrophobic GDL. The condensed water then accumulates and blocks the anode gas channel. In contrast, using hydrophilic anode GDL, some water condensed on channel surfaces may be wicked into the hydrophilic GDL. Therefore, water clogging in the anode gas channel was avoided under similar operating conditions. This finding implies that the hydrophilic anode GDL can alleviate anode channel flooding.

No water droplets were found on the anode GDL surface under any circumstance. This finding clearly demonstrates the different mechanisms of water transport and distribution inside the GDL between the anode and cathode. Water droplets on the channel walls can only be observed in the wetted area of the anode, resulting from water vapor condensation. The sources of water for condensation may come either from water transport through the membrane or from the diminishing anode gas due to hydrogen consumption.

Current density is a controlling parameter for water condensation and liquid water formation in the anode. High current density leads to higher water flux from the anode to cathode by electro-osmotic drag and thus decreases water content in the anode and reduces the tendency for liquid water formation. In addition, elevating the anode plate temperature modestly is an effective method to mitigate anode flooding.

Due to very low rates of water supply into the anode, it takes considerably longer for channel clogging by liquid water to occur.

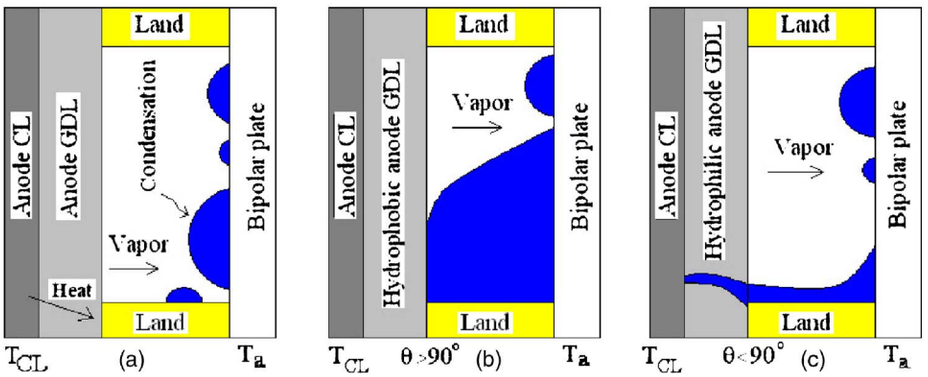

Figure 13. (Color online) Schematic of liquid water formation in the anode channel: (a) water droplets condense on the channel surface, (b) liquid water accumulates and expands in volume, eventually clogging the channel if hydrophobic GDL is used, and (c) liquid water accumulates and subsequently is wicked into a hydrophilic GDL.

Thus, a much longer operational time must be employed in order to capture channel clogging by liquid water on the anode side (i = 0.2 A/cm^2, hydrophobic GDL and $t \geq 60$ min).

Acknowledgments

Financial support of this work by ECEC sponsors is acknowledged. The authors also thank Dr. Richard Steinberger for help in the design of the imaging system and assistance in carrying out experiments and Dr. Jun Li for useful discussions.

The Pennsylvania State University assisted in meeting the publication costs of this article.

References

1. C. Y. Wang, *Chem. Rev. (Washington, D.C.)*, **104**, 4727 (2004).
2. M. M. Mench, Q. L. Dong, and C. Y. Wang, *J. Power Sources*, **124**, 90 (2003).
3. S. H. Ge, X. G. Li, and I. M. Hsing, *J. Electrochem. Soc.*, **151**, B523 (2004).
4. Z. H. Wang, C. Y. Wang, and K. S. Chen, *J. Power Sources*, **94**, 40 (2001).
5. A. Z. Weber and J. Newman, *J. Electrochem. Soc.*, **151**, A326 (2004).
6. U. Pasaogullari and C. Y. Wang, *J. Electrochem. Soc.*, **151**, A399 (2004).
7. K. Tuber, D. Pocza, and C. Hebling, *J. Power Sources*, **124**, 403 (2003).
8. X. G. Yang, F. Y. Zhang, A. L. Lubawy, and C. Y. Wang, *Electrochem. Solid-State Lett.*, **7**, A408 (2004).
9. F. Y. Zhang, X. G. Yang, and C. Y. Wang, *J. Electrochem. Soc.*, **153**, A225 (2006).
10. S. H. Ge and C. Y. Wang, *Electrochem. Solid-State Lett.*, **9**, A499 (2006).
11. S. H. Ge and C. Y. Wang, *Electrochim. Acta*, **52**, 4825 (2007).
12. F. B. Weng, A. Su, C. Y. Hsu, and C. Y. Lee, *J. Power Sources*, **157**, 674 (2006).
13. A. B. Geiger, A. Tsukada, E. Lehmann, P. Vontobel, A. Wokaun, and G. G. Scherer, *Fuel Cells*, **2**, 92 (2002).
14. M. A. Hickner, N. P. Siegel, K. S. Chen, D. N. McBrayer, D. S. Hussey, D. L. Jacobson, and M. Arif, *J. Electrochem. Soc.*, **153**, A902 (2006).
15. K. Teranishi, S. Tsushima, and S. Hirai, *J. Electrochem. Soc.*, **153**, A664 (2006).
16. K. W. Feindel, S. H. Bergens, and R. E. Wasylishen, *J. Am. Chem. Soc.*, **128**, 14192 (2006).
17. P. K. Sinha, P. Halleck, and C. Y. Wang, *Electrochem. Solid-State Lett.*, **9**, A344 (2006).
18. P. K. Sinha, P. P. Mukherjee, and C. Y. Wang, *J. Mater. Chem.*, **17**, 3089 (2007).
19. H. Ju, G. Luo, and C. Y. Wang, *J. Electrochem. Soc.*, **154**, B218 (2007).
20. C. A. Reiser, L. Bregoli, T. W. Patterson, J. S. Yi, J. D. Yang, M. L. Perry, and T. D. Jarvi, *Electrochem. Solid-State Lett.*, **8**, A273 (2005).
21. S. H. Ge and B. L. Yi, *J. Power Sources*, **124**, 1 (2003).
22. S. H. Ge, B. L. Yi, and P. W. Ming, *J. Electrochem. Soc.*, **153**, A1443 (2006).
23. Y. Wang and C. Y. Wang, *Electrochim. Acta*, **50**, 1307 (2005).
24. Y. Wang and C. Y. Wang, *J. Electrochem. Soc.*, **153**, A1193 (2006).
25. G. Luo, H. Ju, and C. Y. Wang, *J. Electrochem. Soc.*, **154**, B316 (2007).